


Chiral morphology in ferrimagnetic Pt/Co/Tb bubble domains

Tao Lin,¹ Xueying Zhang,^{1,2} Nicolas Vernier,³ Xinran Wang,¹ Enxuan Dong ,¹ Chao Chen,¹ Jianteng Niu,¹ Yiming Sun,¹ Liu Yang,¹ Wenhui Zheng,¹ Dan Su,¹ Na Lei,^{1,*} and Weisheng Zhao¹

¹Fert Beijing Institute, MIIT Key Laboratory of Spintronics, School of Integrated Circuit Science and Engineering, Beihang University, Beijing 100191, China

²Beihang-Goertek Joint Microelectronics Institute, Qingdao Research Institute, Beihang University, Qingdao 266000, China and Beihang Hangzhou Innovation Institute (Yuhang), Beihang University, Hangzhou 311121, China

³Laboratoire Lumière, Matière et Interfaces, Université Paris-Saclay, Orsay 91405, France



(Received 15 July 2022; revised 12 October 2022; accepted 13 October 2022; published 7 November 2022)

The Dzyaloshinskii-Moriya interaction (DMI) is a key factor in chiral spin textures and has great potential in spintronics-based applications. The asymmetric bubble domain expansion under an in-plane magnetic field is a common method for DMI evaluation. However, abnormal bubble expansions occur occasionally in the creep regime, which may lead to deviations in the DMI evaluation, implying various physical phenomena in domain wall (DW) kinetics. In this study, DMI evaluation of ferrimagnetic Pt/Co/Tb trilayers was conducted via DW motion in the creep and flow regimes, where the in-plane fields of minimum DW velocities are significantly different for 1.5 nm Co. The accuracy of the extracted DMI effective field in the flow regime was confirmed by Brillouin light scattering measurements, where the DMI coefficient was approximately 1 mJ/m². In the creep regime, a typical flattened bubble shape was observed; accordingly, the dominant direction of the DW motion velocity changes with increasing the in-plane magnetic fields. Based on the bubble morphology and DW anisotropy energy analyses, we attributed the bubble expansion phenomena in the creep regime to the vertical Bloch lines. Our study provides alternatives for a better understanding of DW kinetics in DMI evaluations, which is essential for spin-texture applications.

DOI: [10.1103/PhysRevB.106.184407](https://doi.org/10.1103/PhysRevB.106.184407)

I. INTRODUCTION

Recently, remarkable progress has been made regarding chiral spintronics, where ideal device performance and new functionalities can be achieved [1]. Chiral spin textures, such as chiral domain walls (DWs) and skyrmions that are typically generated from the Dzyaloshinskii-Moriya interaction (DMI) induced by spin-orbit coupling, can improve their spin torque driven motion efficiency [2–4]. Because of their kinetic characteristics, these spin textures are ideal candidates for future information carriers in spintronic applications [5–8]. Accurately determining the DMI is crucial for designing magnetic layers. In addition to methods based on spin waves [9–11] and spin-orbit torques [12,13], asymmetric DW motion is a common method utilized for DMI evaluation [14–16]. The DMI effective fields can be extracted from the curves of the DW velocity versus the in-plane magnetic field (v - H_{ip} curves) based on the asymmetric expansion of bubble domains. However, some abnormal phenomena have been reported for DW motion in the creep regime, which implies that complex physics is involved. For instance, high in-plane magnetic fields obstruct rather than assist DW motion in Pt/Co/GdO_x [6], and a change of dominant direction of DW velocity is observed in v - H_{ip} curves with an increase of the in-plane magnetic field [17]. Thus, chiral damping has been proposed to explain

these abnormal behaviors [6,18,19]. However, because the kinematic properties of DWs are often extracted from the expansions of bubble domains, these bubbles may also be related to the abnormal behaviors.

For example, the bubble domain morphologies can provide insight into the underlying physics. Regarding Co/Ni multilayer films, Lau *et al.* reported the chiral shapes of bubble domains in the creep regime [20,21]. The chiral bubbles include two typical shapes; one is a teardrop and the other has a flattened boundary like the letter D. The Wulff construction model can explain the teardrop shape appropriately, whereas an extremely large DW anisotropy is required to fit the D shape [20]. The evolution of DW morphologies was highlighted in a subsequent study [22]. Possible vertical Bloch lines (VBLs) have been referred to theoretically [23]; nevertheless, experimental investigations remain lacking. Aiming to provide alternatives to the chiral bubbles, experiments of multilayers with the D-shaped bubble domains are performed in this study.

Here, the DMI evaluation of Pt/Co/Tb was analyzed based on DW motion in the creep and flow regimes, and the extracted nominal DMI effective fields exhibited large deviations. The Brillouin light scattering results confirm DMI extraction in the flow regime. Additionally, we found that the deviation in DMI evaluations comes from the D-shaped bubble morphologies in the creep regime, for which the VBLs are presumably the physical origin. Thus far, experimental studies are needed to understand the VBLs in chiral bub-

*Corresponding author: na.lei@buaa.edu.cn

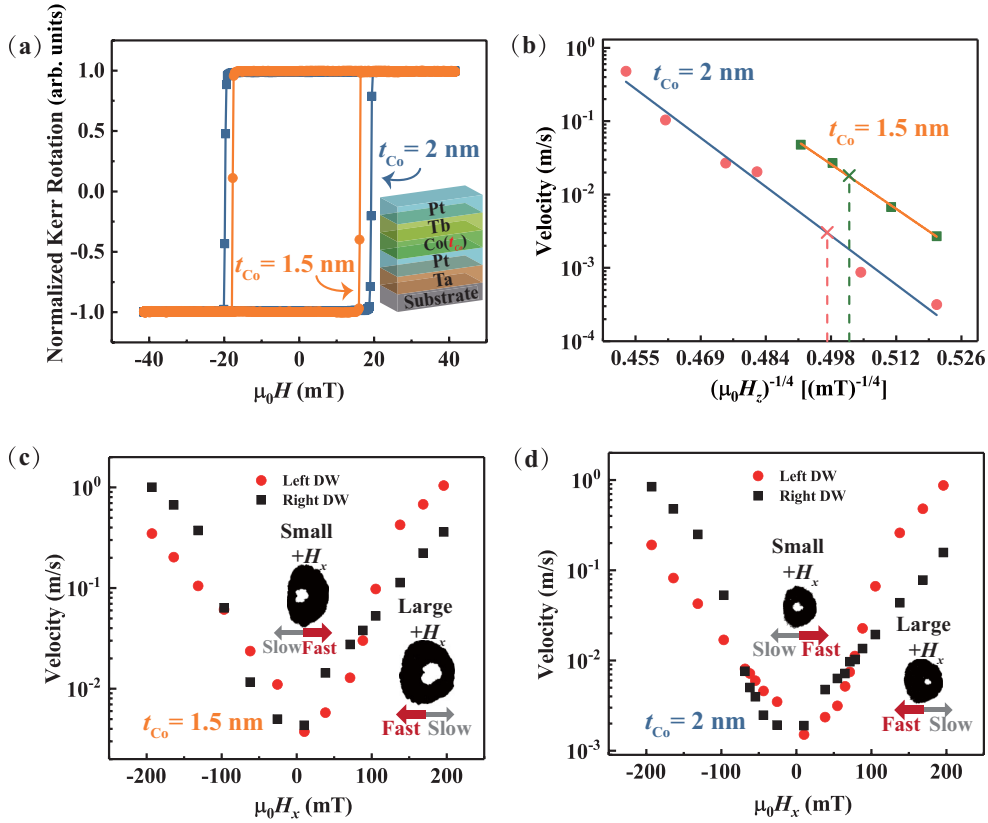


FIG. 1. Magnetic properties and evaluation of DMI based on DW motion in the creep regime of ferrimagnetic Pt/Co/Tb multilayer. (a) Schematic of the Pt/Co/Tb sample structures and their out of plane magnetic hysteresis loops measured by MOKE. (b) DW velocities with various perpendicular magnetic fields H_z for the samples with Co layer thickness $t_{Co} = 1.5$ nm (green squares) and $t_{Co} = 2$ nm (pink dots), respectively. The in-plane magnetic field is zero in this experiment, and the crosses indicate the H_z used in (c),(d). (c),(d) DW velocities vary with in-plane magnetic fields H_x under a fixed H_z . The red dots (black squares) correspond to left (right) DW velocities ($+H_x$ is pointing right). The insets denote the domain images under small and large $+H_x$, respectively.

ble domains and how they affect DMI evaluations based on asymmetric bubble expansion. This study provides the DMI coefficient of the Pt/Co/Tb trilayer, which is beneficial for ferrimagnetic spin-texture optimization [24–27]. The results of this study may provide a reference for studying chirality in chiral spin textures, which is crucial for the development of chiral spintronics. This study may also offer further insight into chiral DW kinetics and underlying physical phenomena.

II. RESULTS AND DISCUSSION

A. Sample preparation and DMI evaluation through creeping DWs

The samples are prepared by magnetron sputtering with a base pressure lower than 10^{-7} Torr, where the structure is Si substrate/Ta(3)/Pt(5)/Co(1.5 and 2)/Tb(1)/Pt(3); all thicknesses are reported in nm. Figure 1(a) depicts the hysteresis loops of the samples measured using the magneto-optical Kerr effect (MOKE) in a polar configuration. The saturation magnetization and effective magnetic anisotropy of the sample with Co 1.5 nm are presented in Fig. S1 in the Supplemental Material [28]. The saturation magnetization is 1.1×10^6 A/m, which is slightly smaller than that of pure Co because of the antiferromagnetic coupling between Co and Tb layers. Moreover, the magnetic anisotropy energy is

approximately 0.15 MJ/m³, which is reasonable compared to that of other Pt/Co-based multilayers [29].

To evaluate the DMI effective field in the Pt/Co/Tb trilayer, asymmetric DW motion under in-plane magnetic fields was investigated in the creep regime [15]. Figure 1(b) demonstrates the relationship between the logarithm-scale DW velocity and $\mu_0 H_z^{-1/4}$. Note that only a perpendicular magnetic field H_z is applied in the case represented in Fig. 1(b). Observe that in the measurement range of $\mu_0 H_z$ (14.66 – 16.22 mT for $t_{Co} = 1.5$ nm and 13.57 – 23.71 mT for $t_{Co} = 2$ nm), a decent linear relation can be obtained. According to the creep law [15,30],

$$v(H_z) = v_0 \exp[-\kappa H_z^{-1/4}], \quad (1)$$

where v_0 is a velocity prefactor and κ is a function of H_z . DW motion in the creep regime follows the linear relation between $\ln v$ and $H_z^{-1/4}$ [15,30]. The perpendicular magnetic fields are kept constant at 15.76 and 16.38 mT for $t_{Co} = 1.5$ and 2 nm, respectively, indicated by the crosses marked in Fig. 1(b). By varying the in-plane magnetic fields, DW velocities of left/right DWs are extracted, which show parabolic behavior with a tilted axis of symmetry depicted in Figs. 1(c) and 1(d). Moreover, with increasing amplitude of the in-plane magnetic fields, the dominant direction of the DW motion velocity

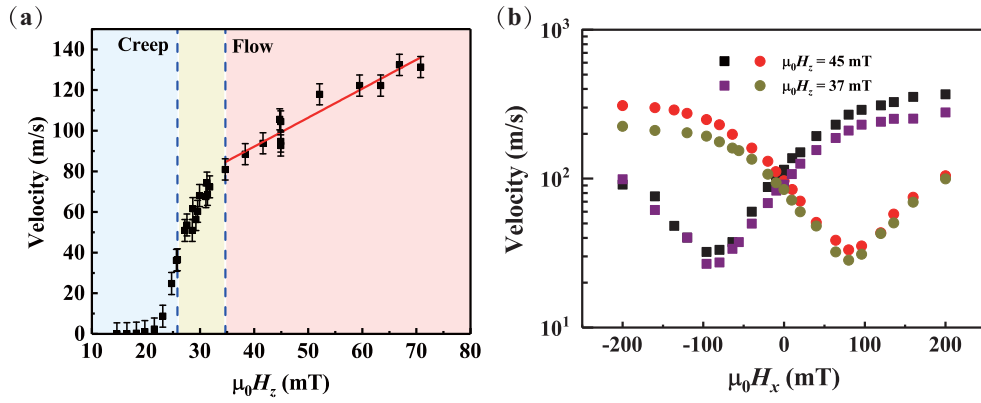


FIG. 2. Determination of DMI effective field in the Pt/Co(1.5)/Tb multilayers through DW motion in the flow regime. (a) Determination of creep and flow regimes of DW motion with perpendicular magnetic fields. The red line denotes a linear fit of velocities in the flow regime. (b) DW motion velocities with continuous in-plane magnetic fields (H_x) and perpendicular pulse magnetic fields (H_z) applied simultaneously. Perpendicular magnetic fields are indicated in the legends and square (circle) points indicate the $+H_x$ ($-H_x$) directions of DW motion.

changes at a certain in-plane magnetic field. The changed fields are approximately 100 and 70 mT for $t_{\text{Co}} = 1.5$ and 2 nm, respectively. A similar DW velocity-changing behavior has been reported and explained through chiral damping [17], while the analysis of the corresponding chiral morphologies and DMI evaluation is missed. Furthermore, although the exact value of the in-plane magnetic field showing the minimum velocity is difficult to determine, the data point shows the minimum velocity around $\mu_0 H_x = 10$ mT. Considering the symmetry in the DW velocity versus in-plane magnetic field behavior, and in-plane magnetic field step length in measurement, observe that both the $t_{\text{Co}} = 1.5$ and 2 nm samples show velocity minima of $|\mu_0 H_x|$ between 0 and 25.67 mT. Take this range as $|\mu_0 H_{\text{DMI}}|$ into Eq. (2) [15],

$$H_{\text{DMI}} = D/(\mu_0 M_s \lambda), \quad (2)$$

where M_s is the saturation magnetization and λ is the DW width, $\lambda = \sqrt{\frac{A}{K}}$, A is the exchange constant, and K is the anisotropy constant. Here we use $M_s = 1.1 \times 10^6$ A/m, $K = 0.15$ MJ/m³, and $A = 1.3 \times 10^{-11}$ J/m [31]; the calculated DMI coefficient is in the range of 0 – 0.26 mJ/m². These values are much smaller than those of other Pt/Co-based multilayers, such as Pt/Co/Ta and Pt/Co/MgO [32,33]. Therefore, the extracted $|\mu_0 H_x|$ might deviate from the DMI effective field, and further experiments are needed to determine the DMI effective field in Pt/Co/Tb trilayers.

B. Determination of DMI effective field

Considering the low in-plane magnetic fields of minimum DW velocities and the change of dominant DW velocity direction without changing H_x direction in the creep regime, we further evaluate the DMI of the Pt/Co(1.5)/Tb trilayer in the flow regime. The details of the device fabrication and experimental measurements are provided in Fig. S2 in the Supplemental Material [28]. The kinetics of the DW motion under perpendicular magnetic fields was studied. The creep, depinning, and flow regimes are marked by different colored regions in Fig. 2(a). The critical fields of ~ 25.8 and ~ 34.7 mT for creep and flow regimes are determined by linear fitting between DW velocity and applied fields

(logarithmic scale in the creep regime as shown in Fig. S3 in the Supplemental Material [28]). The asymmetric DW motion velocity in the flow regime induced by in-plane magnetic fields was studied under constant perpendicular field pulses ($\mu_0 H_z = 37$ and 45 mT), and the results are shown in Fig. 2(b). The asymmetric DW motion velocity curves follow a typical parabolic shape [18]; the velocity minima occur at $\mu_0 H_x$ around 90 mT, which is significantly larger than that in the creep regime. Furthermore, no changes in the dominant DW velocity direction with increasing the in-plane magnetic fields can be observed, showing great deviation compared to the DW motion in the creep regime [Fig. 1(c)]. Considering the asymmetry of the curves and the step length of the in-plane magnetic field, the DMI effective field is determined as 88 ± 8 mT. Therefore, the DMI constant is evaluated to be $|D| = 0.90 \pm 0.08$ mJ/m² through Eq. (1), which is consistent with the reported value of Pt/Co-based multilayers [34].

As there is a disagreement between the DMI constant measured in the creep and flow regimes of DW motion, Brillouin light scattering (BLS), based on spin wave dispersion [35], has been used to validate the DMI constant evaluation. This interfacial asymmetry leads to Stokes and anti-Stokes shifts in the frequency spectra. Figure 3(a) shows a representative BLS spectrum of a Pt/Co(1.5)/Tb multilayer under an in-plane magnetic field of 700 mT, where the incident light corresponds to $k = 15.18 \mu\text{m}^{-1}$. Solid lines are fittings of the Stokes and anti-Stokes components of the spectrum, and dashed lines are their inversions. The nonreciprocal behavior of the spin wave can be observed, and the frequency shifts with the wave vectors by varying the scattering angles are extracted, as shown in Fig. 3(b). Error bars represent the fitting errors of the peaks. According to $\Delta f = \frac{2\gamma}{\pi M_s} Dk$ [36], where $\frac{\gamma}{2\pi} = 30.35$ GHz/T in Pt/Co multilayers [37], the DMI constant is evaluated to be $D = -1.07 \pm 0.05$ mJ/m² through linear fitting where its sign is also determined in the measurement. Compared with the DW motion measurements, the DMI evaluation in the flow regime is consistent with the BLS measurements, indicating that the DW asymmetric motion in the flow regime is more reliable than in the creep regime [34].

By comparison with the BLS results, we confirm that the DMI effective field in the flow regime is reasonable. Studies

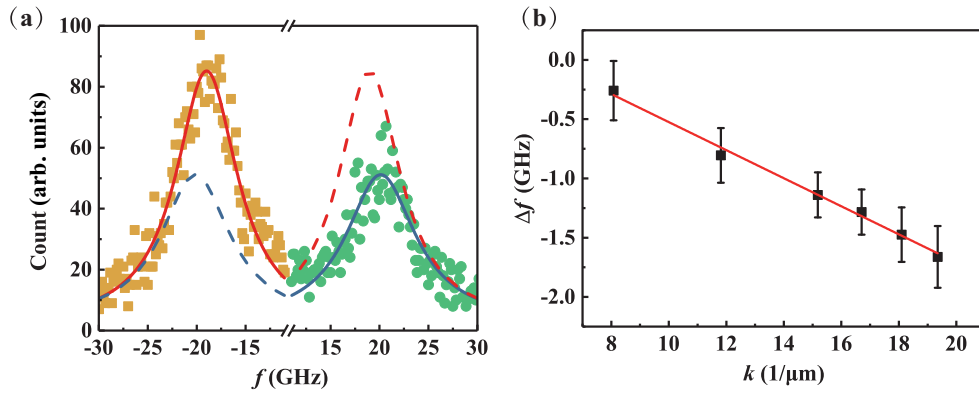


FIG. 3. BLS measurements for the Pt/Co(1.5)/Tb multilayers. (a) BLS spectrum with scattering angle at 40° and wave vector $k = 15.18 \mu\text{m}^{-1}$. Yellow (green) dots are Stokes (anti-Stokes) components and blue (red) solid lines are the Lorentz peak fit of them. The dashed lines are fitted lines with an inverted k to clearly show the frequency shifts. (b) Frequency shifts (Δf) against wave vectors. The red line is a linear fit of the results.

have also conducted DMI measurements in the flow regime of DWs [6,18]. Typically, DW velocities decrease when H_x approaches the H_{DMI} in the DMI measurement because DWs tend to transform from Néel to Bloch configurations. However, the DW velocities reach a minimum far before the H_{DMI} and show a swapping asymmetry around the H_{DMI} in the creep regime. Therefore, we investigated the morphologies of the bubble domains to analyze the possible mechanisms for the blocking/accelerating DW motions in the Pt/Co/Tb multilayers.

C. Morphologies of chiral bubble domains in DMI evaluation

The evolution of the domain expansion is shown in Fig. 4(a), where the domains of the Co 1.5/2 nm samples are shown in the upper and lower panels, respectively. The inner light gray areas are the domains initially nucleated by a pulsed

perpendicular magnetic field and the dark areas show domain expansion driven by both perpendicular and in-plane magnetic fields. To precisely measure the DW velocities, the total pulse duration (t) was controlled to maintain the bubble domains in proper sizes with different in-plane magnetic fields. The positive in-plane magnetic field points to the right, as shown in Fig. 4(b). Both samples showed similar DW motions and domain bubble morphologies. When the in-plane magnetic fields are small, the right DW moves faster than the left DW, and the domains have a bubble shape. With increasing in-plane magnetic fields, the left DW moves significantly faster, and the edges of the domains tend to be flattened with a noncircular shape, as shown in the second column of Fig. 4(a). Note that the bubbles with flattened edges are still shown as an in-plane magnetic field near the crossing point in Figs. 1(c) and 1(d), where the DW velocities in both directions are equal. Then, the left DW moves faster than the right one, while the domains

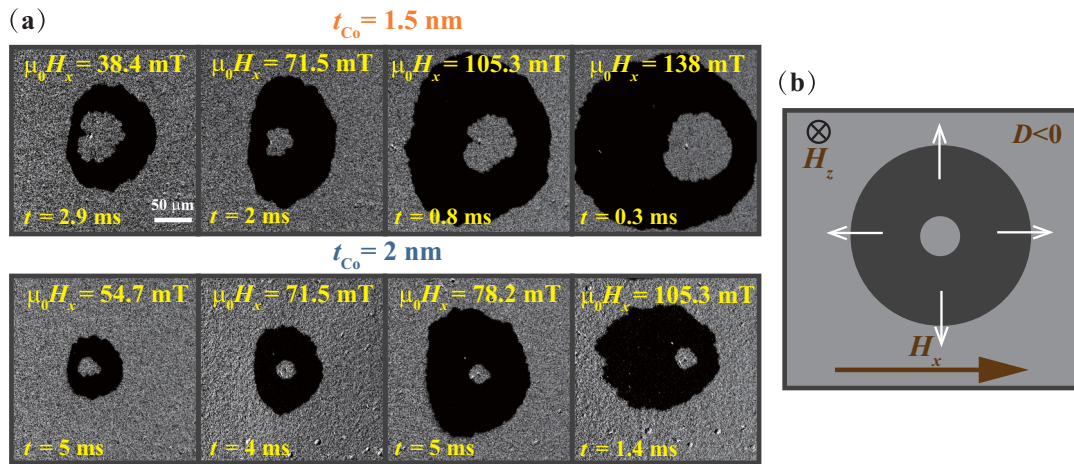


FIG. 4. Domains in the asymmetric DW motion measurement shown in Figs. 1(c) and 1(d). (a) Domain images observed through Kerr microscope; light areas inside bubble domains are nucleation created by perpendicular pulse field. Then both in-plane and perpendicular magnetic fields are applied to enlarge the bubble domains (dark areas). In-plane magnetic fields (H_x) are continuous as marked in the pictures. Perpendicular pulse fields ($\mu_0 H_z$) to drive the DWs are 15.76 mT (upper row, Co 1.5 nm sample) and 16.38 mT (lower row, Co 2 nm sample); total pulse durations (t) are indicated in the pictures. (b) Schematic picture of the magnetic fields and DMI-induced DW chirality (white arrows) of the bubble domains.

TABLE I. Magnetic properties (total magnetic layer thickness t_{mag} , exchange constant A , anisotropy constant K , saturation magnetization M_s , and DW anisotropy K_D) of some reported sample structures with chiral morphologies of bubble domains.

Sample structure (thickness in nm)	t_{mag} (nm)	A ($\times 10^{-11}$ J/m)	K ($\times 10^5$ J/m ³)	M_s (kA/m)	K_D ($\times 10^4$ J/m ³)	Reference
Si/TaN(3)/Pt(2.5)/[Co(0.2)/Ni(0.6)] ₂ /Co(0.2)/Ta(0.5)/TaN(3)	1.8	1.0	3.0	600	3.0	[20]
Si/TaN(3)/Pt(3.5)/Pt _x Ir _{1-x} (1.2)/[Co(0.2)/Ni(0.6)] ₂ /Co(0.2)/Ta(0.8)/TaN(6)	1.8	1.0	4.2	645	2.1	[21]
Sub/MgO(2)/Pt(4)/Co(0.32)/[Pd(0.34)/Co(0.32)] ₃ /MgO(2)/SiO ₂ (3)	1.28	1.0	2.4	880	2.1	[39]
Pt/Co ₉₀ Fe ₁₀ /Pt (simulation)	0.6	1.3	15	1353	5.2	[23]
Si/Ta(3)/Pt(5)/Co(1.5)/Tb(1)/Pt(3)	1.5	1.3	1.5	1100	2.7	This work

tend to be round again with a large in-plane bias magnetic field. Figure 4(b) shows the chirality of the DW inferred from the sign of the DMI, where the white arrows indicate the in-plane magnetization component in the DW. From the BLS measurement, we can conclude that the DMI coefficient is negative in the Pt/Co/Tb trilayer, which is mainly from the Pt/Co interface owing to the strong spin-orbit coupling.

In Co/Ni multilayers, a phenomenon similar to that of noncircular domains has been reported [20]. The Wulff construction model was proposed to explain the evolution of domain expansion by varying the DW anisotropy energy. DW anisotropy is the energy density difference between the Bloch wall and Néel wall, where the Néel wall forms as a result of DMI [18,20]. To realize noncircular domains with flattened edges in that model, a very large DW anisotropy energy ($\sim 10^5$ J/m³) must be considered. Here, we calculate the DW anisotropy constant K_D in our Pt/Co(1.5 nm)/Tb multilayer based on the DW anisotropy equation [13,38],

$$K_D = N_x \mu_0 M_s^2 / 2, \quad (3)$$

$$N_x = t_{\text{mag}} \ln(2) / (\pi \lambda), \quad (4)$$

where t_{mag} denotes the thickness of the magnetic layer [13,38]. The calculated K_D for Pt/Co/Tb is 2.7×10^4 J/m³, which is one order lower than that used in the energetic chiral bubble model [20]. Furthermore, we calculated and summarized the DW anisotropy energies for the material systems reported with the chiral morphologies of the bubble domains in Table I. Note that A is chosen as 1.0×10^{-11} J/m if it is not introduced in the references in Table I, and the magnetic properties are from different structures (skyrmion and DMI samples) in [39]. Clearly, the DW anisotropies are of the same order of $\sim 10^4$ J/m³, which is far below the value required to form a chiral-morphology bubble with a flattened edge. Thus, microscopic explanations of noncircular bubble domains are still required.

The flattened edge domains have been reported theoretically by considering the VBLs to block the DW motion with experimentally comparable K_D [23], where typical ripple DWs are shown. These results are highly consistent with the chiral morphologies in the Pt/Co/Tb bubble domains we observed, which can be clearly seen in Fig. 4 for both 1.5 and 2 nm Co. Therefore, we can analyze the VBLs from their kinetic behaviors, although highly technical conditions are required to directly observe VBLs in spin textures. In addition, VBLs must be considered in defect-dominated disordered

films [40,41]. Moreover, the DW velocity reaches a minimum far before the value of H_{DMI} , as shown in Fig. 1, which indicates the blocking of VBLs plays a more important role than the addition of the simple one-dimensional (1D) model to extract H_{DMI} in the creep regime. In the presence of DMI, the pairs of VBLs move at different velocities and collide owing to energy splitting [42]. In this process, D-shaped bubble domains are gradually formed, where VBLs block DW motion in the flattened edges. VBLs are a viewpoint from magnetic microstructures in the DWs for the underlying physics in addition to modeling and calculations. Even though the change of dominant direction of DW velocities with increasing the in-plane magnetic fields is not well understood from the viewpoint of VBLs, the kinetics of DWs is complicated but worth studying because of the underlying rich physics, especially in the creep regime. In addition, the DMI is a fundamental basis for chiral spin textures, and an explicit evaluation of the DMI in materials with noncircular bubble domains is essential for chiral spintronics. In multilayers with DMI, VBLs should be emphasized, especially in the chiral morphologies in bubble domain expansion.

III. CONCLUSION

DMI is fundamentally important in magnetic chiral textures, and it is crucial to properly evaluate the DMI experimentally. The puzzling behavior of DW motion in the creep regime raises doubts regarding the DMI measurement method based on bubble expansion. In this study, we focus on the DMI evaluation of ferrimagnetic Pt/Co/Tb multilayer films. The DW motions in the creep and flow regimes are analyzed, and the bubble morphologies in the creep regime are investigated. The experimental results and comparison of magnetic properties provide evidence to support the theory that VBLs in DWs are the physical origin of chiral bubble morphologies. BLS is applied to clarify the exact DMI in samples with complicated DW motions. In addition, this study establishes a link between bubble domain morphologies and their effects on DMI effective field extractions. The obtained results have a certain reference value for modifying and explaining DMI measurement methods in chiral multilayer materials, where DMI is an important part of spintronics.

ACKNOWLEDGMENT

This study was supported by the National Natural Science Foundation of China (Grants No. 52061135105 and No. 12074025).

- [1] S.-H. Yang, R. Naaman, Y. Paltiel, and S. S. P. Parkin, *Nat. Rev. Phys.* **3**, 328 (2021).
- [2] S.-H. Yang, *Appl. Phys. Lett.* **116**, 120502 (2020).
- [3] A. Hrabec, M. Belmeguenai, A. Stashkevich, S. M. Chérif, S. Rohart, Y. Roussigné, and A. Thiaville, *Appl. Phys. Lett.* **110**, 242402 (2017).
- [4] J. Miltat, S. Rohart, and A. Thiaville, *Phys. Rev. B* **97**, 214426 (2018).
- [5] A. V. Khvalkovskiy, V. Cros, D. Apalkov, V. Nikitin, M. Krounbi, K. A. Zvezdin, A. Anane, J. Grollier, and A. Fert, *Phys. Rev. B* **87**, 020402 (2013).
- [6] M. Vaňatka, J.-C. Rojas-Sánchez, J. Vogel, M. Bonfim, M. Belmeguenai, Y. Roussigné, A. Stashkevich, A. Thiaville, and S. Pizzini, *J. Phys.: Condens. Matter* **27**, 326002 (2015).
- [7] S. Li, A. Du, Y. Wang, X. Wang, X. Zhang, H. Cheng, W. Cai, S. Lu, K. Cao, B. Pan *et al.*, *Sci. Bull.* **67**, 691 (2022).
- [8] L. Wang, H. Cheng, P. Li, L. W. van Hees Youri, Y. Liu, K. Cao, R. Lavrijsen, X. Lin, B. Koopmans, and W. Zhao, *Proc. Natl. Acad. Sci. USA* **119**, e2204732119 (2022).
- [9] K. Di, V. L. Zhang, H. S. Lim, S. C. Ng, M. H. Kuok, X. Qiu, and H. Yang, *Appl. Phys. Lett.* **106**, 052403 (2015).
- [10] K. Di, V. L. Zhang, H. S. Lim, S. C. Ng, M. H. Kuok, J. Yu, J. Yoon, X. Qiu, and H. Yang, *Phys. Rev. Lett.* **114**, 047201 (2015).
- [11] V. L. Zhang, K. Di, H. S. Lim, S. C. Ng, M. H. Kuok, J. Yu, J. Yoon, X. Qiu, and H. Yang, *Appl. Phys. Lett.* **107**, 022402 (2015).
- [12] C.-F. Pai, M. Mann, A. J. Tan, and G. S. D. Beach, *Phys. Rev. B* **93**, 144409 (2016).
- [13] T. Dohi, S. Fukami, and H. Ohno, *Phys. Rev. B* **103**, 214450 (2021).
- [14] A. Hrabec, N. A. Porter, A. Wells, M. J. Benitez, G. Burnell, S. McVitie, D. McGrouther, T. A. Moore, and C. H. Marrows, *Phys. Rev. B* **90**, 020402 (2014).
- [15] R. Soucaille, M. Belmeguenai, J. Torrejon, J. V. Kim, T. Devolder, Y. Roussigné, S. M. Chérif, A. A. Stashkevich, M. Hayashi, and J. P. Adam, *Phys. Rev. B* **94**, 104431 (2016).
- [16] S.-G. Je, D.-H. Kim, S.-C. Yoo, B.-C. Min, K.-J. Lee, and S.-B. Choe, *Phys. Rev. B* **88**, 214401 (2013).
- [17] C. K. Safeer, M.-A. Nsibi, J. Nath, M. S. Gabor, H. Yang, I. Joumard, S. Auffret, G. Gaudin, and I.-M. Miron, *Nat. Commun.* **13**, 1192 (2022).
- [18] D.-H. Kim, D.-Y. Kim, S.-C. Yoo, B.-C. Min, and S.-B. Choe, *Phys. Rev. B* **99**, 134401 (2019).
- [19] E. Jué, C. K. Safeer, M. Drouard, A. Lopez, P. Balint, L. Buda-Prejbeanu, O. Boulle, S. Auffret, A. Schuhl, A. Manchon *et al.*, *Nat. Mater.* **15**, 272 (2016).
- [20] D. Lau, V. Sundar, J.-G. Zhu, and V. Sokalski, *Phys. Rev. B* **94**, 060401(R) (2016).
- [21] D. Lau, J. P. Pellegren, H. T. Nembach, J. M. Shaw, and V. Sokalski, *Phys. Rev. B* **98**, 184410 (2018).
- [22] J. P. Pellegren, D. Lau, and V. Sokalski, *Phys. Rev. Lett.* **119**, 027203 (2017).
- [23] B. Sarma, F. Garcia-Sanchez, S. A. Nasser, A. Casiraghi, and G. Durin, *J. Magn. Magn. Mater.* **456**, 433 (2018).
- [24] K. Cai, Z. Zhu, J. M. Lee, R. Mishra, L. Ren, S. D. Pollard, P. He, G. Liang, K. L. Teo, and H. Yang, *Nat. Electron.* **3**, 97 (2020).
- [25] Y. Hirata, D.-H. Kim, S. K. Kim, D.-K. Lee, S.-H. Oh, D.-Y. Kim, T. Nishimura, T. Okuno, Y. Futakawa, H. Yoshikawa *et al.*, *Nat. Nanotechnol.* **14**, 232 (2019).
- [26] S. Woo, K. M. Song, X. Zhang, Y. Zhou, M. Ezawa, X. Liu, S. Finizio, J. Raabe, N. J. Lee, S.-I. Kim *et al.*, *Nat. Commun.* **9**, 959 (2018).
- [27] S. Pöllath, T. Lin, N. Lei, W. Zhao, J. Zweck, and C. H. Back, *Ultramicroscopy* **212**, 112973 (2020).
- [28] See Supplemental Material at <http://link.aps.org/supplemental/10.1103/PhysRevB.106.184407> for measurement of magnetic properties for the Co 1.5 nm Pt/Co/Tb sample, experimental setup for evaluating DMI through domain wall motion in the flow regime, and determination of the creep regime in evaluation of the DMI effective field in the flow regime.
- [29] L.-R. Yu, X.-L. Xu, Y.-L. Jia, X. Geng, X.-J. Ma, Y.-F. Ma, Y.-H. Zan, C. Feng, and J. Teng, *Rare Met.* **40**, 2855 (2021).
- [30] S. Lemerle, J. Ferré, C. Chappert, V. Mathet, T. Giamarchi, and P. Le Doussal, *Phys. Rev. Lett.* **80**, 849 (1998).
- [31] P. E. Tannenwald and R. Weber, *Phys. Rev.* **121**, 715 (1961).
- [32] J. Yun, D. Li, B. Cui, X. Guo, K. Wu, X. Zhang, Y. Wang, J. Mao, Y. Zuo, and L. Xi, *J. Phys. D: Appl. Phys.* **51**, 155001 (2018).
- [33] A. Cao, X. Zhang, B. Koopmans, S. Peng, Y. Zhang, Z. Wang, S. Yan, H. Yang, and W. Zhao, *Nanoscale* **10**, 12062 (2018).
- [34] K. Shahbazi, J.-V. Kim, H. T. Nembach, J. M. Shaw, A. Bischof, M. D. Rossell, V. Jeudy, T. A. Moore, and C. H. Marrows, *Phys. Rev. B* **99**, 094409 (2019).
- [35] H. T. Nembach, J. M. Shaw, M. Weiler, E. Jué, and T. J. Silva, *Nat. Phys.* **11**, 825 (2015).
- [36] M. Belmeguenai, J. P. Adam, Y. Roussigné, S. Eimer, T. Devolder, J. V. Kim, S. M. Cherif, A. Stashkevich, and A. Thiaville, *Phys. Rev. B* **91**, 180405(R) (2015).
- [37] M. Belmeguenai, Y. Roussigné, S. M. Chérif, A. Stashkevich, T. Petrisor, M. Nasui, and M. S. Gabor, *J. Phys. D: Appl. Phys.* **52**, 125002 (2019).
- [38] R. Lavrijsen, D. M. F. Hartmann, A. van den Brink, Y. Yin, B. Barcones, R. A. Duine, M. A. Verheijen, H. J. M. Swagten, and B. Koopmans, *Phys. Rev. B* **91**, 104414 (2015).
- [39] S. D. Pollard, J. A. Garlow, J. Yu, Z. Wang, Y. Zhu, and H. Yang, *Nat. Commun.* **8**, 14761 (2017).
- [40] J. Leliaert, B. Van de Wiele, A. Vansteenkiste, L. Laurson, G. Durin, L. Dupré, and B. Van Waeyenberge, *J. Appl. Phys.* **115**, 17D102 (2014).
- [41] J. Leliaert, B. Van de Wiele, A. Vansteenkiste, L. Laurson, G. Durin, L. Dupré, and B. Van Waeyenberge, *J. Appl. Phys.* **115**, 233903 (2014).
- [42] Y. Yoshimura, K.-J. Kim, T. Taniguchi, T. Tono, K. Ueda, R. Hiramatsu, T. Moriyama, K. Yamada, Y. Nakatani, and T. Ono, *Nat. Phys.* **12**, 157 (2016).